Solid solution softening in single crystalline metal nanowires studied by atomistic simulations

Zuoyong Zhang and Chuang Deng[*]
Department of Mechanical Engineering, University of Manitoba, Winnipeg MB R3T 5V6, Canada

Solid solution strengthening is a common method used in physical metallurgy to increase the strength of metals. However, it is also possible for solute atoms to reduce the strength of metals, known as the solid solution softening effect. In this paper, atomistic simulations were carried out using molecular dynamics and Monte Carlo simulations to explore the softening phenomenon in single crystalline metal nanowires (MNWs) of different alloy systems. It was found that, for single crystalline MNWs, softening is more prominent than strengthening when solute atoms are introduced, which contrasts with the solid solution strengthening that is usually observed in bulk metals. The reduction of unstable stacking fault energy, increase in atomic size misfit, and solute clustering are responsible for this phenomenon, as they facilitate the surface dislocation nucleation in the alloyed nanowires. Additionally, while the nanowire diameter, orientation, surface segregation, and chemical short-range ordering all influence the yield strength, they do not alter the overall softening trend. It is assumed that the softening mechanisms uncovered in this paper are applicable to metallic structures whose yielding is determined by dislocation nucleation.

I. INTRODUCTION

Alloying with solute atoms is a classical approach for improving the strength of metals. However, it has been shown that solute atoms can also reduce the strength of certain metals, a phenomenon known as *solid solution softening* (SSS) [1]. This effect was reported in the 1960s, when Arsenault [2] studied the solid solution effects in body-centered cubic (bcc) metals. He proposed that SSS is caused by the reduction in Peierls stress due to the presence of solute atoms, and his theoretical calculations were consistent with experimental results. This theory was further validated by Cheng *et al.* [3], who explored the effect of small additions of Al into a Cantor CoCrFeMnNi high-entropy alloy (HEA) resulting in softening, while Al additions into CoCrNi medium-entropy alloys (MEAs) caused hardening [4,5]. Another reason behind SSS is local lattice distortion, which is attributed to the facilitation of dislocation nucleation in dislocation-starved alloys, even though it can impede the dislocation motion [6]. Medvedeva *et al.* [7–9] asserted that SSS in Mo-based alloys is caused by electron structures. They stated that the addition of elements with excess electrons (e.g., Pt, Ir, Os, or Re) as solute atoms into the bcc Mo matrix induces SSS owing to the reduction in stacking fault energy (SFE) and shear stress on the atomic scale, which facilitates double-kink nucleation and enhances dislocation mobility. On the contrary, the addition of solute atoms such as Hf would lead to a hardening effect due to the lack of electrons in the outer shell.

Although the strength of the metals can be reduced by solute atoms, there are potential improvements in terms of toughness and ductility. For instance, the toughness of Ni-Co alloy nanoparticles can be improved with higher Co concentration [10], and small additions of Al into the Cantor HEA can soften strength but enhance ductility [3]. Moreover, SSS can improve the ductility of bcc tungsten-based alloys [11] and face-centered cubic (fcc) silver-based alloys [12]. To improve the ductility of hexagonal close-packed (hcp) Mg-based alloys, the SSS strategy has been used to show that yttrium is a potential solute element by significantly reducing the SFE and inducing softening while enhancing ductility [13].

Previous work into SSS mainly focused on polycrystals since conventional bulk metals are mostly polycrystalline. In recent decades, single crystalline metal nanowires (MNWs) have emerged as an important class of metallic structures with unique mechanical properties [14–17] that can be easily fabricated via various methods [18–21] and developed for numerous applications [22–25]. However, the softening phenomenon and the corresponding mechanisms caused by solute atoms in single crystalline metals, or more specifically single crystalline MNWs, remain largely unknown. In recent studies, Bisht *et al.* [10] and Sharma *et al.* [26] found SSS in defect-free Ni-Co and Ni-Fe single crystalline nanoparticles through both experiments and molecular dynamics (MD) simulations. This is different from the strengthening effect caused by the addition of Co solute atoms into the Ni-based superalloys [27]. Their research showed that softening was associated with solute-induced premature dislocation nucleation at sites with local stress concentration in Ni-Fe and the local spatial variations of resolved shear stress in Ni-Co nanoparticles, respectively. It is unclear whether the softening mechanisms based on polycrystalline bulk metals or single crystalline metal nanoparticles still work, or if alloying-induced softening mechanisms can be observed in single crystalline MNWs.

In this paper, atomistic simulations were used to explore the substitutional solute effects on the yield strength of various

[*]Corresponding author: Chuang.Deng@umanitoba.ca
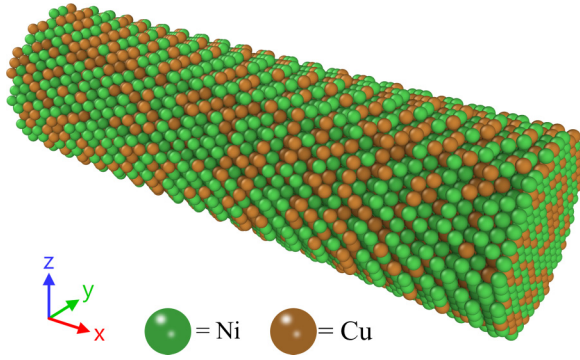
FIG. 1. Atomistic structure of the cylindrical Ni-Cu metal nanowire (MNW) model. The green spheres represent nickel atoms, while the brown ones represent copper atoms, which are randomly distributed throughout the MNW. The MNW axis is oriented parallel to the *x* axis.

single crystalline MNWs at room temperature. Different alloy systems (i.e., Ni-Cu, Ni-Co, Cu-Ag, NiFe-Cu, CoCrNiFe-Cu, and Al-Mg) were chosen to perform uniaxial tensile tests. Hybrid MD/Monte Carlo (MC) simulations were employed to investigate the possible solute distribution effects on softening phenomenon. The SFE and atomic size misfit were also calculated to evaluate the sources of softening in yield strength in single crystalline MNWs. Several softening mechanisms were found and discussed.

II. COMPUTATIONAL METHODS

A. Tools and MNW model construction

All atomistic simulations in this paper were performed by using the open-source software package LAMMPS [28], while MNW models were constructed with Atomsk [29]. All initial models were created by randomly substituting the corresponding host atoms with solute ones. For atomic visualization, OVITO [30] was employed. Structure identification was done using the common neighbor analysis method [31], and dislocation analysis was done with the dislocation extraction algorithm [32], which is integrated into the toolkit OVITO.

To study the SSS phenomenon of single crystalline MNWs, several different alloy systems were chosen. Ni-Cu was selected for its unlimited solubility, while Ni-Co was chosen for comparison with the work by Bisht *et al.* [10]. The NiFe-Cu MEA and CoCrNiFe-Cu HEA systems were employed to investigate the possible chemical effects on SSS. Additionally, the immiscible Cu-Ag alloy system and the widely used Al-Mg alloy system were chosen for their comprehensive engineering applications. All MNWs were cylindrical and had a length-to-diameter ratio of ∼3.2, like Refs. [33,34], and a diameter of ∼4 nm, varying slightly based on the lattice constants of the alloy system. Here, ⟨111⟩-oriented Ni-Cu MNWs of larger size ($D = 8$ nm) were also tested to examine possible size dependence of SSS effects. The Ni-Cu MNW model is illustrated in Fig. 1, with the axial direction of the MNW parallel to the *x* axis. Three different orientations ⟨111⟩, ⟨110⟩, and ⟨100⟩ were used for the Ni-Cu MNWs, while all other MNWs were ⟨111⟩ oriented except the ⟨0001⟩-oriented Mg-Al MNWs with an hcp structure. The solute concen-

TABLE I. List of MNWs and the corresponding solute concentration range, structure, and orientation. The element after the dash indicates the solute element.

MNWs	Solute content (at. %)	Structure	Orientation
Ni-Cu	0–100	fcc	⟨111⟩, ⟨110⟩, and ⟨100⟩
Ni-Co	1–60	fcc	⟨111⟩
(NiFe)-Cu	12–48	fcc	⟨111⟩
(CoCrNiFe)-Cu	12–48	fcc	⟨111⟩
Cu-Ag	1–10	fcc	⟨111⟩
Ag-Cu	1–10	fcc	⟨111⟩
Al-Mg	2–12	fcc	⟨111⟩
Mg-Al	2–12	hcp	⟨0001⟩

trations and orientations for different MNWs are listed in Table I.

B. Uniaxial tensile simulations

Uniaxial tensile tests were conducted on single crystalline MNWs made of Ni-Cu, Ni-Co, Cu-Ag, NiFe-Cu, and CoCrNiFe-Cu, to investigate the potential SSS effects. To accurately simulate the atomic interactions of the Ni-Cu alloy system, the embedded-atom method (EAM) potential developed by Onat and Durukanoğlu [35] was used. The Ni-Co system was evaluated by the many-body angular-dependent interatomic potential developed by Purja *et al.* [36], which is the same potential used by Bisht *et al.* [10]. The Cu-Ag system was described by the EAM potential developed by Williams *et al.* [37], while the quinary EAM potential for the HEA system CoCrFeNiCu developed by Deluigi *et al.* [38] was used for the NiFe-Cu MEA and CoCrNiFe-Cu HEA MNWs.

Periodic boundary conditions were applied along the axial direction (i.e., the *x* direction) of the MNWs, while the other directions were free. The timestep was 1 fs. To relax the MNW structures, the microcanonical ensemble (NVE) was applied to each MNW model at room temperature (300 K) for 50 ps, followed by an isothermal-isobaric ensemble (NPT) at 300 K and setting zero pressure in the axial direction for an additional 50 ps. Uniaxial deformation was then applied to each MNW model with a constant strain rate of 10^9 s^{-1}, while the temperature was kept at room temperature by using the canonical ensemble (NVT). The atomic stress was calculated using the Virial theorem [39], and snapshots were captured during the deforming for postobservation and analysis. We also conducted uniaxial tensile simulations of Ni-Cu MNWs at different strain rates (10^8 and 10^7 s^{-1}) and different temperatures (100 and 400 K) to better comprehend the temperature and strain rate dependence of SSS.

C. Hybrid MD/MC simulations

Hybrid MD/MC simulations were performed in the Ni-Cu, Ni-Co, Cu-Ag, and Al-Mg alloy systems to investigate the possible influence of solute distribution on SSS. The interatomic interactions for the Ni-Cu, Ni-Co, and Cu-Ag alloy systems were modeled by using the same potentials as

described in Sec. II. The EAM potential developed by Mendelev *et al.* [40] was used to evaluate the interactions in the Al-Mg alloy system. Initially, periodic boundary conditions were imposed on all directions of each MNW. The timestep was set to 1 fs, and the structure of each MNW model was optimized using the conjugate gradient algorithm, followed by a structural relaxation by the NPT ensemble at 300 K and zero pressure for 50 ps. After that, the hybrid MD/MC simulations were implemented by utilizing the Metropolis algorithm [41], with a smaller timestep (0.1 fs) to ensure the system remained stable. In total, 5 million steps were run for sufficient atomic exchanges, and the MC atom swap was invoked every 10 MD steps. During the hybrid MD/MC procedure, the temperature was kept at 300 K by the NVT ensemble, while the pressure was maintained at zero in all directions by the Berendsen barostat [42]. After the hybrid MD/MC relaxation, the periodic boundary condition was kept in the MNW axial direction while changing the rest of the directions to free boundary conditions. The timestep was also changed to 1 fs. The resulting models of hybrid MD/MC simulations were then subject to tensile testing by using the same procedure as previously described in Sec. II.

D. SFE calculations

It is reported that the unstable SFE (γ_{USF}) in fcc metals is the energy barrier corresponding to the nucleation of $\frac{1}{6}\langle 112 \rangle$ partial dislocations [43]. To calculate the SFE for each alloy system, the step-by-step rigid shifting method described in Refs. [44,45] was used. Rectangular supercells were generated by Atomsk [29] oriented in the $\langle 112 \rangle$, $\langle 110 \rangle$, and $\langle 111 \rangle$ directions with 24 000 atoms and 10 {111} planes in each model. The atomic sites were populated randomly by the host or solute atoms. We also calculated the SFE of a Ni-Cu system with orderly distributed Cu atoms (see Fig. S1(a) in the Supplemental Material [46]) to understand the solute distribution effects on γ_{USF}.

III. COMPUTATIONAL RESULTS

A. SSS in MNWs with randomly distributed solutes

The uniaxial tensile stress-strain curves of $\langle 111 \rangle$-oriented Ni-Cu MNWs are shown in Fig. 2(a), demonstrating obvious yielding points without strain-hardening phenomenon. Similarly, the stress-strain curves of other alloy systems behaved in the same manner. The relationship between the uniaxial tensile yield strength and the solute concentration of the Ni-Cu, Cu-Ag, NiFe-Cu, CoCrNiFe-Cu, and Ni-Co MNWs with randomly distributed solutes are illustrated in Figs. 2(b)–2(e), respectively. Figure 2(f) demonstrates that MNWs without any defects are formed by random dislocation nucleation from the free surface, which is unlike the results reported by Wu *et al.* [47], where yielding occurred at the artificial surface defects. For the Ni-Cu MNWs, the yield strength monotonically decreased with higher Cu concentrations for all three different orientations [Fig. 2(b)], indicating that the Ni-Cu MNWs were continuously softened in their yield strength by adding more Cu atoms regardless of the axial orientation. This trend also persisted for $\langle 111 \rangle$-oriented Ni-Cu MNWs with larger sizes (e.g., $D = 8$ nm). Thus, only the $\langle 111 \rangle$ axial direction and
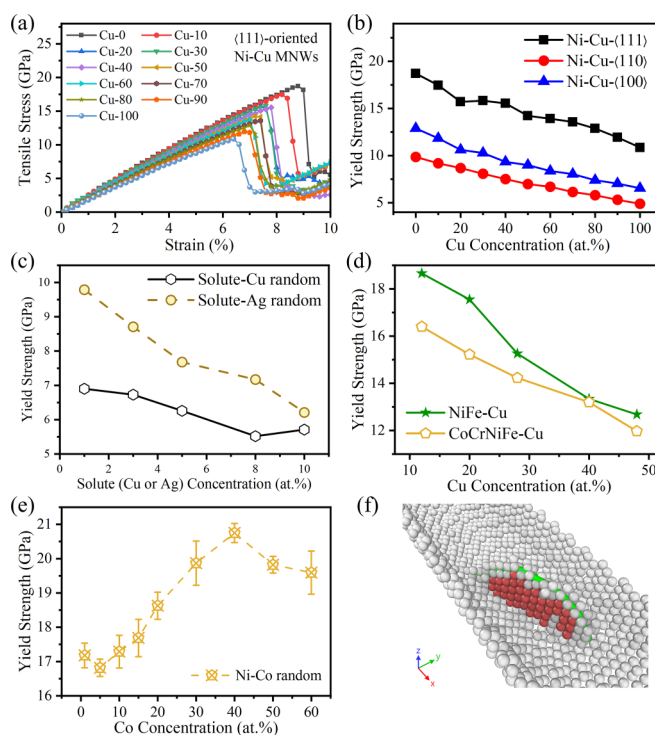
FIG. 2. Tensile yielding results of metal nanowires (MNWs) with randomly distributed solute atoms in (a) $\langle 111 \rangle$-oriented Ni-Cu MNWs, (b) $\langle 111 \rangle$-, $\langle 110 \rangle$-, and $\langle 100 \rangle$-oriented Ni-Cu MNWs, (c) Cu-Ag and Ag-Cu MNWs, (d) NiFe-Cu medium-entropy alloy (MEA) and CoCrNiFe-Cu high-entropy alloy (HEA) MNWs, and (e) Ni-Co MNWs. The results in (e) are obtained by averaging over five different Co atomic distributions due to the existence of the transition points, and the error bars represent the standard deviation. There are no error bars for other alloy systems since no softening-to-strengthening or strengthening-to-softening points can be observed. (f) illustrates the yielding by dislocation nucleation from the free surface. The dark red spheres represent the stacking fault with the hexagonal close-packed (hcp) structure. The gray spheres represent other structures.

$D = \sim 4$ nm were used to investigate the SSS effects in most other alloy systems. Moreover, Fig. S2 in the Supplemental Material [46] demonstrates that, while the yield strength can be affected by varying strain rates and temperatures, the SSS phenomenon remains unchanged. Therefore, only 300 K and 10^9 s^{-1} were used for the other alloy systems.

Similarly, SSS was observed in the $\langle 111 \rangle$-oriented Cu-Ag and Ag-Cu MNWs by increasing either the solute Ag or Cu concentrations [Fig. 2(c)]. The yield strength varied between 6.9 and 5.52 GPa when Cu changed from 1 to 10 at. % and from 9.79 GPa at Ag-1 at. % to 6.21 GPa at Ag-10 at. %. Furthermore, the NiFe-Cu MEA and CoCrNiFe-Cu HEA MNWs showed monotonic softening behaviors in yield strength by increasing the Cu concentration [Fig. 2(d)]. The CoCrNiFe-Cu HEA MNW exhibited a consistently lower yield strength than the corresponding NiFe-Cu MEA MNW for Cu concentrations <40 at. %, implying that the addition of Co and Cr can soften the yield strength of the MNWs.

The yield strength vs solute concentration behavior of Ni-Co MNWs was more complex, as a small addition of Co atoms
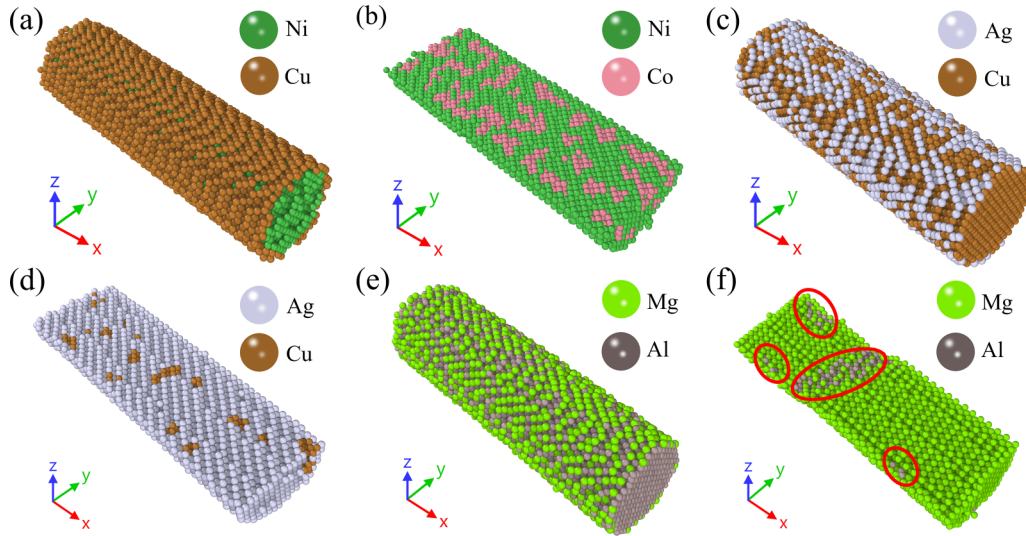
FIG. 3. Structures after hybrid molecular dynamics (MD)/Monte Carlo (MC) simulations for (a) Ni-Cu, (b) Ni-Co, (c) Cu-Ag, (d) Ag-Cu, (e) Al-Mg, and (f) Mg-Al alloy metal nanowires (MNWs). (f) shows that Al-rich phases (precipitates) are formed in the circled regions after hybrid MD/MC relaxation when the Al concentration is higher than ∼8 at. %. The MNWs in (b), (d), and (f) were sliced to show the solute distribution in the core of the MNWs.

softened the yield strength from 17.58 GPa at Co-1 at. % to 16.53 GPa at Co-5 at. %, followed by a strengthening up to 20.64 GPa at 40 at. % and then another softening regime. There were two critical Co concentrations, 5 and 40 at. %, which marked the transition points of softening-to-strengthening-to-softening in yield strength for the Ni-Co MNWs, a behavior different from that observed in the Ni-Co nanoparticles reported by Bisht *et al.* [10].

B. SSS in MNWs with hybrid MD/MC simulations

Hybrid MD/MC simulations were used to investigate the mechanical behaviors of several alloy MNWs and understand the solute distribution effects (or the widely reported chemical short-range ordering effects) on the softening phenomena. The resulting structures are shown in Fig. 3. It is evident that Cu atoms tend to segregate to the surface of the Ni-Cu alloy MNWs [Fig. 3(a)], forming a core-shell structure with Ni atoms at the core. This surface segregation phenomenon has been previously evidenced through both theoretical calculations [48] and experiments [49], especially for heavily alloyed Ni-Cu metals.

Similarly, a surface segregation can be seen in Cu-Ag [Fig. 3(c)] and Al-Mg [Fig. 3(e)] MNWs. A different result was observed in Ni-Co MNWs, where random Co clusters form inside the MNWs [Fig. 3(b)], with higher Co concentration resulting in heavier Co clustering. Ag-Cu MNWs also tend to form small Cu clusters [Fig. 3(d)]. No secondary phases were seen in the fcc MNWs. However, hcp Mg-Al MNWs [Fig. 3(f)] formed Al-rich precipitates, indicating that they cannot be treated as a single-phase solid solution.

The yielding of MNWs relaxed by the hybrid MD/MC simulations was caused by the nucleation of partial dislocation from the free surface upon tensile loading, which is expected because they are still defect-free single crystalline MNWs, even with surface segregation or solute clustering having occurred. Figure 4 presents the tensile yield strength

for each alloy MNW with hybrid MD/MC simulations. For ⟨111⟩-oriented Ni-Cu MNWs with surface segregation, the yield strength showed the same monotonic softening trend as for the ones with random solute distribution [Fig. 4(a)], implying that SSS in Ni-Cu MNWs was insensitive to the chemical short-range ordering. However, the hybrid MD/MC relaxation dramatically affected the mechanical behaviors of the Ni-Co MNWs. The yield strength of Ni-Co MNWs with hybrid MD/MC relaxation was consistently lower than that of their counterparts with random solute distribution when the Co concentration was between 1 and 40 at. %, as seen in Fig. 4(b). This is likely related to the clustering of Co atoms, which caused a shift in the softening-to-
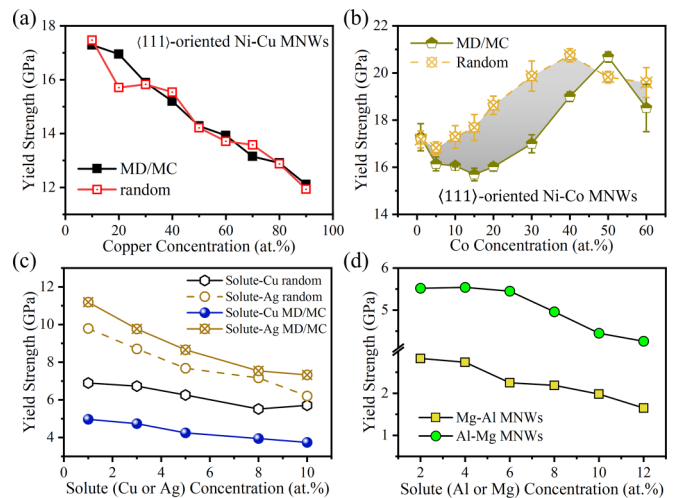
FIG. 4. Tensile yield strength of metal nanowires (MNWs) subjected to hybrid molecular dynamics (MD)/Monte Carlo (MC) simulations for (a) ⟨111⟩-oriented Ni-Cu MNWs, (b) ⟨111⟩-oriented Ni-Co MNWs, (c) Cu-Ag and Ag-Cu MNWs, and (d) Mg-Al and Al-Mg MNWs.

TABLE II. Summary of energy barriers for γ_{USF} and γ_{ISF} in Ni-Cu alloy systems predicted by the EAM potential developed by Onat and Durukanoğlu [35]. The 0 and 100 at. % Cu concentrations refer to pure Ni and Cu cases, respectively.

Cu content (at. %)	0	10	20	30	40	50	60	70	80	90	100
γ_{USF}, mJ/m^2	273.3	262.4	249.3	238.1	229.1	214.7	201.6	190.9	178.1	166.7	158.5
γ_{ISF}, mJ/m^2	126.0	116.8	105.4	93.9	87.2	74.8	66.3	61.9	53.1	48.2	45.2

strengthening transition point from Co-5 at. % to Co-15 at. % and a postponement of the strengthening-to-softening point from Co-40 at. % to Co-50 at. %.

The results of the immiscible Cu-Ag MNWs with hybrid MD/MC relaxation demonstrate that the yield strength can be softened by increasing the solute concentration of either Ag or Cu [Fig. 4(c)]. When Ag was the solute, the yield strength decreased from 11.19 GPa at Ag-1 at. % to 7.33 GPa at Ag-10 at. %, and when Cu was the solute, it reduced from 4.97 to 3.74 GPa. Interestingly, the Cu-Ag MNWs with hybrid MD/MC relaxation were strengthened compared with the corresponding random MNWs, indicating that the surface segregation of Ag atoms or the chemical long-range ordering of Cu atoms can reinforce the yield strength. However, the Ag-Cu MNWs with hybrid MD/MC relaxation were dramatically softened compared with their random counterpart. In the case of Al-Mg MNWs, the yield strength remained almost unchanged when the solute Mg concentration was <6 at. % [Fig. 4(d)]. After that, the yield strength was reduced from 5.45 GPa at Mg-6 at. % to 4.26 GPa at Mg-12 at. %, indicating that the softening in yield strength of Al-Mg MNWs only occurred when the solute concentration was higher than the critical value 6 at. %, which is different from the other alloy systems.

C. Influence of solute concentration on SFE

The fault energies for different alloy systems are listed in Tables II–VI, where γ_{USF} refers to the energy barrier for the stacking fault formation and γ_{ISF} is the intrinsic SFE when a perfect stacking fault is formed. Results show that pure Ni has the highest γ_{USF} (273.3 mJ/m^2), which is consistent with the result reported by Siegel [50], and pure Cu has the lowest γ_{USF} (158.5 mJ/m^2), which is consistent with the value reported by Mishin *et al.* [51]. The γ_{USF} values are monotonically reduced by increasing the Cu concentration in the Ni-Cu alloy models.

However, γ_{USF} for the Ni-Co alloy system increases from 300.2 mJ/m^2 at Co-1 at. % to 473.4 mJ/m^2 at Co-50 at. %, then slightly drops to 470.4 mJ/m^2 at Co-60 at. %, as shown in Table III. The γ_{USF} values of the NiFe-Cu MEA and CoCrNiFe-Cu HEA systems are also monotonically reduced from 366.6 and 280.5 mJ/m^2 to 302.3 and 256.1 mJ/m^2 by increasing the Cu concentration from 12 to 48 at. %, respec-

tively, as seen in Table IV. As for the Cu-Ag alloy system, γ_{USF} decreases from 112.8 to 110.0 mJ/m^2 by increasing the concentration of solute Ag from 1 to 10 at. %. However, the γ_{USF} values dramatically decrease from 160.0 to 144.0 mJ/m^2 when Cu is the solute and its concentration increases from 1 to 10 at. %, as shown in Table V. Lastly, for the Al-Mg alloy system, γ_{USF} is also reduced by increasing the solute concentration, which can be seen in Table VI.

IV. DISCUSSIONS

A. SFE-induced softening

Previous results have indicated that Ni-Cu MNWs exhibit similar SSS trends and yielding mechanisms regardless of the axial orientation or surface segregation. Therefore, the softening mechanisms in Ni-Cu MNWs will be discussed using the ⟨111⟩-oriented ones with randomly distributed solute atoms as representatives.

It has been suggested that atomic friction stress [3,10] and atomic lattice distortion [6] may also affect the yielding behavior of fcc metals. However, this is contradicted by the observed softening in Ni-Cu MNWs, as atomic friction stress can only increase the yield strength when the material is yielded by dislocation motion. Moreover, the atomic size misfit can be calculated using Eqs. (1) and (2) [52]:

$$\delta = \sqrt{\sum_{i=1}^{n} c_i \left(1 - \frac{r_i}{\bar{r}}\right)^2}, \qquad (1)$$

$$\bar{r} = \sum_{i=1}^{n} c_i r_i, \qquad (2)$$

where n indicates the number of atom species; i represents the ith element; c_i is the atomic fraction of the ith element; r_i is the radius of the ith component; and $\bar{r}$ is the average atomic radius of the alloy system, which is evaluated by Eq. (2). The atomic radii for Co, Cr, Fe, Ni, and Cu are taken from Ref. [53], which are 125, 128, 126, 124, and 125 pm, respectively. The calculated atomic size misfit for the Ni-Cu alloy system increases from 0% at Cu-0 at. % to 1.58% at Cu-50 at. %, then gradually decreases to 0% at Cu-100 at. %. This transition in atomic size misfit (i.e., increase then decrease) is inconsistent with the monotonic trend of SSS in Ni-Cu MNWs when the

TABLE III. Summary of energy barriers for γ_{USF} and γ_{ISF} in Ni-Co alloy systems predicted by the EAM potential developed by Purja *et al.* [36].

Co content (at. %)	1	5	10	15	20	30	40	50	60
γ_{USF}, mJ/m^2	300.2	311.1	333.1	359.7	382.6	417.0	466.5	473.4	470.4
γ_{ISF}, mJ/m^2	136.2	147.0	172.9	204.0	229.3	263.5	326.8	318.5	326.9

TABLE IV. Summary of energy barriers for γ_{USF} and γ_{ISF} in the NiFe-Cu MEA and CoCrNiFe-Cu HEA systems predicted by the EAM potential developed by Deluigi *et al.* [38].

Cu content (at. %)		12	20	28	40	48
γ_{USF}, mJ/m^2	NiFe-Cu	366.6	351.5	344.1	324.4	302.3
	CoCrNiFe-Cu	280.5	277.8	268.3	257.3	256.1
γ_{ISF}, mJ/m^2	NiFe-Cu	85.7	78.9	77.9	70.9	59.6
	CoCrNiFe-Cu	60.8	61.9	55.8	54.2	55.2

TABLE VI. Summary of energy barriers for γ_{USF} and γ_{ISF} for the Al-Mg alloy system predicted by the EAM potential developed by Mendelev *et al.* [40].

Mg content (at. %)	2	4	6	8	10	12
γ_{USF}, mJ/m^2	211.2	204.4	196.9	190.1	185.2	177.2
γ_{ISF}, mJ/m^2	126	125.7	125.1	125	124.6	125.4

Cu concentration increases, suggesting the atomic size misfit and the associated lattice distortion should not be the main cause of SSS in Ni-Cu MNWs. For the NiFe-Cu MEA and CoCrNiFe-Cu HEA systems, the calculated atomic size misfit is also negligibly small, ranging from 1.08 to 1.27%.

As depicted in Fig. 5(a), both the yield strength and γ_{USF} are monotonically reduced when the Cu concentration increases, despite some minor fluctuations. Figure 5(b) shows a linear relationship between the yield strength and γ_{USF} of the $\langle 111 \rangle$-oriented Ni-Cu MNWs, with R^2 up to 0.96. This indicates that the weakening of $\langle 111 \rangle$-oriented Ni-Cu NWs is caused by the reduction of γ_{USF} when the Cu concentration increases. This is reasonable since the yielding in all Ni-Cu MNWs is initiated by the nucleation of $\frac{1}{6}\langle 112 \rangle$ partial dislocations on the free surface. Similarly, the γ_{USF} values for the NiFe-Cu and CoCrNiFe-Cu MNWs are also linearly related to the yield strength, as shown in Fig. 5(b), with R^2 values 0.91 and 0.93, respectively. Thus, the softening in the NiFe-Cu MEA and CoCrNiFe-Cu HEA systems can also be attributed to the reduction of γ_{USF} caused by an increase in solute concentration.

The behavior of the SSS in Ni-Cu after hybrid MD/MC simulations can also be explained by the reduction of γ_{USF} with higher Cu concentrations. This phenomenon demonstrates that γ_{USF} is not affected by the atomic distribution of solute on the slip planes but is dependent on the overall composition of the slip planes (see Fig. S1(b) in the Supplemental Material [46]). Thus, even though the Cu atoms migrate to the outer shells of the MNWs after hybrid MD/MC relaxation, the composition on the slip planes remains unchanged compared with the random conditions. This can be used to explain the yield strength of the Ni-Cu MNWs or the softening phenomenon that does not seem to be affected by the surface segregation of Cu atoms after hybrid MD/MC simulations. Additionally, the yield strength of the Ni-Cu MNWs follows the rule of mixture; as the Ni concentration increases, the yield strength increases monotonically. This is because Ni-Cu is a typical isomorphous system, and the atomic size misfit can

be negligible, making the yield strength generally follow the trend of γ_{USF}.

B. Atomic size misfit-induced softening

SSS can be observed in the Cu-Ag alloy system with or without hybrid MD/MC relaxation [Fig. 4(c)]. When Cu or Ag is the solute, higher concentrations always reduce the yield strength of the alloy MNWs, which is different from the monotonic softening in Ni-Cu MNWs only when the solute atoms are Cu. The atomic size misfit for the Cu-Ag alloy system has been calculated using Eqs. (1) and (2) with the atomic radii of Cu 128 pm and Ag 144 pm from Ref. [53]. The calculated results are presented in Figs. 6(a) and 6(b) for solute-Ag and solute-Cu cases, respectively. The atomic size misfit increases with the solute concentration for both cases, and the yield strength reduces with higher solute concentrations, which follows the propensity that atomic size misfit aids the nucleation of the first partial dislocation in single crystalline metals [6].

The correlations between the yield strength and atomic size misfit for both cases are shown in Fig. 6(c). The yield strength is highly dependent on the atomic size misfit for both the solute-Cu and Ag cases, with R^2 values as high as 0.97 and 0.99, respectively. As mentioned, γ_{USF} for the solute-Cu case only varies between 112.8 and 110.0 mJ/m^2, indicating that the change in γ_{USF} by adding the Cu solutes in Ag is small, and the influence on the yield strength of Ag-Cu MNWs should be negligible. Therefore, the softening in the solute-Cu case can be attributed to the increase of atomic size misfit when increasing the Cu concentration, which is referred to as the atomic size misfit-induced softening. For the solute-Ag case, the yield strength is also positively related to γ_{USF} with the R^2 value up to 0.88, as shown in Fig. 6(d). Therefore, both the atomic size misfit and γ_{USF} have contributed to the softening phenomenon in the solute-Ag case, with the atomic size misfit dominating due to a higher R^2 value.

TABLE V. Summary of energy barriers for γ_{USF} and γ_{ISF} in the Cu-Ag alloy system predicted by the EAM potential developed by Williams *et al.* [37].

Solute (Cu or Ag) content (at. %)		1	3	5	8	10
γ_{USF}, mJ/m^2	Solute-Cu	112.8	112.5	111.8	110.8	110.0
	Solute-Ag	160.0	150.9	149.5	148.4	144.0
γ_{ISF}, mJ/m^2	Solute-Cu	21.1	19.7	18.1	16.5	14.5
	Solute-Ag	49.4	45.3	42.9	42.3	38.5
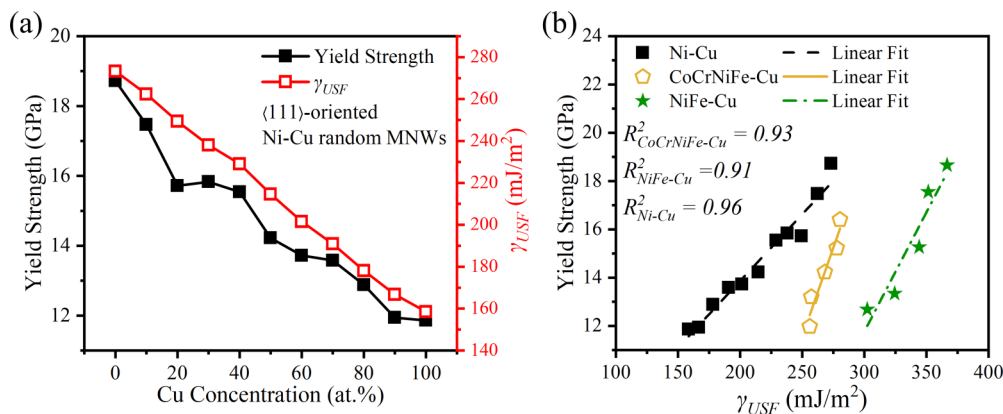
FIG. 5. (a) The yield strength and γ_{USF} vs Cu concentration in Ni-Cu metal nanowires (MNWs). (b) The yield strength vs γ_{USF} for the Ni-Cu, NiFe-Cu medium-entropy alloy (MEA), and CoCrNiFe-Cu high-entropy alloy (HEA) systems.

C. Misfit-SFE combined softening

The atomic size misfit for the Al-Mg alloy system has also been calculated using Eqs. (1) and (2) with atomic radii for Al 143 pm and Mg 160 pm taken from Ref. [53]. Figure 7(a) illustrates the relationship between atomic size misfit and yield strength with Mg concentration, where the atomic size misfit increases with the Mg concentration. However, a small addition of solute Mg atoms into the Al matrix has little effect on the yield strength of the Al-Mg MNWs, which is attributed to the reduction of host-solute interactions resulting from surface segregation of Mg atoms after hybrid MD/MC simulations. The yield strength remains steady initially, followed by a dramatic softening when Mg concentration exceeds 6 at. %. This can be divided into two regions: Region-1 (steady yield strength) and Region-2 (dramatic softening), as seen in Figs. 7(b) and 7(c). In Region-1, both the

atomic size misfit and γ_{USF} have little influence on the yield strength R^2 values being only 0.46 and 0.55, respectively.

By contrast, the yield strength in Region-2 is strongly related to both the atomic size misfit and γ_{USF} with R^2 of 0.98 and 0.96, respectively. The atomic size misfit has a negative relationship with the yield strength, whereas γ_{USF} has a positive relationship. This can be explained by the fact that Mg atoms segregate to the surface, resulting in an enhanced atomic misfit at the free surface where partial dislocations form. Furthermore, the addition of Mg atoms reduces the partial dislocation nucleation energy barriers (γ_{USF}). Thus, the enhanced atomic size misfit and reduced γ_{USF} both contribute to the softening of yield strength. Consequently, the softening mechanism in the Al-Mg MNWs can be described as misfit-SFE combined softening.

Surface segregation can be observed in both Ni-Cu and Al-Mg MWNs after hybrid MD/MC simulations, although
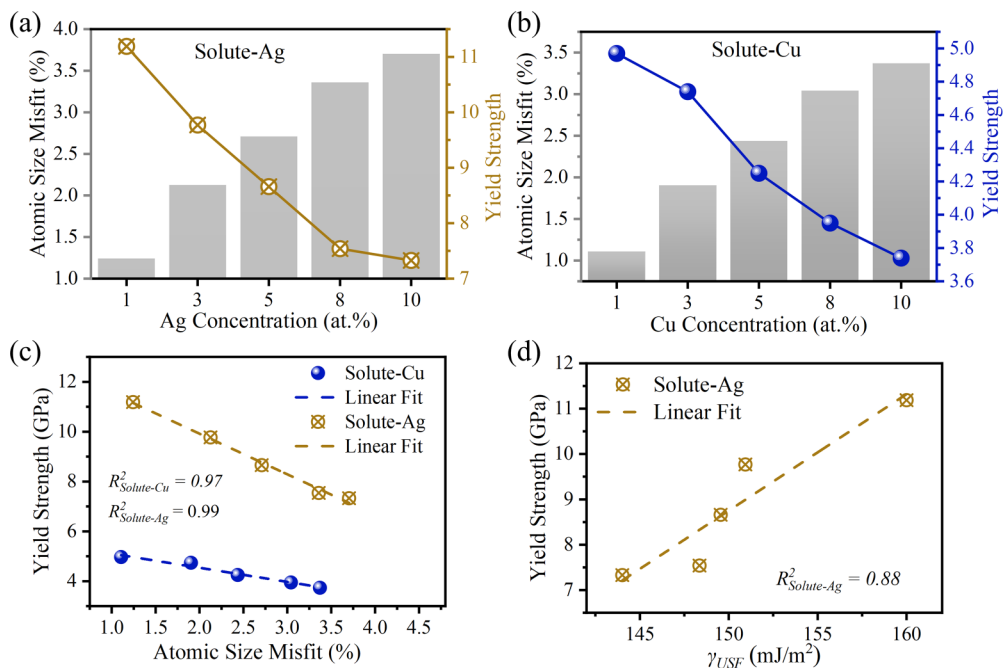
FIG. 6. The atomic size misfit in (a) Ag-Cu and (b) Cu-Ag metal nanowires (MNWs). (c) and (d) illustrate the yield strength vs atomic size misfit and γ_{USF} in Cu-Ag and Ag-Cu MNWs, respectively.
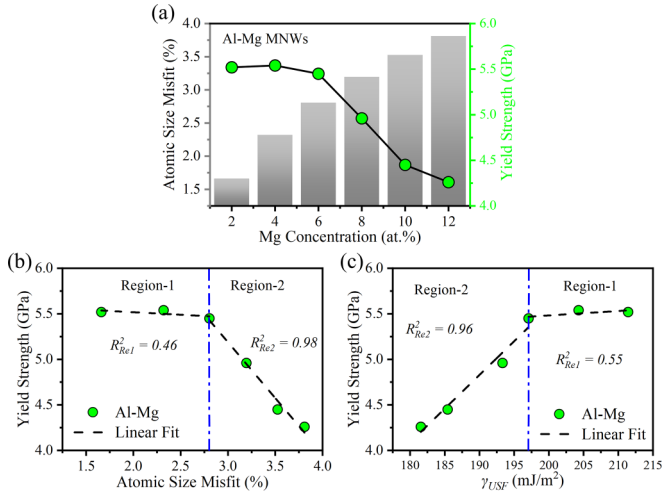
FIG. 7. (a) Atomic size misfit and yield strength vs the solute Mg concentration in Al-Mg metal nanowires (MNWs). (b) and (c) illustrate the correlation between the atomic size misfit and γ_{USF} with yield strength. The coefficient R^2_{Re1} and R^2_{Re2} represent the R^2 values for the linear fit in Region-1 and Region-2, respectively.

the softening mechanisms are significantly different. This difference can be attributed to two main factors: atomic size misfit and solute concentration. While the Cu and Ni atomic sizes are almost the same, eliminating any stress concentration due to impurities, the size misfit between Al and Mg is more pronounced, leading to greater stress concentration and dislocation nucleation. Additionally, the Mg content typically ranges from 2 to 12 at. %, while Cu content ranges from 10 to 90 at. %. It was observed that, in the low solute concentration region (Mg < 6 at. %), Mg atoms cannot occupy the outer layer comprehensively, resulting in host-solute interactions that are too weak to affect the yielding of the Al-Mg MNWs (see Fig. S3 in the Supplemental Material [46]). This is evident from Region-1 in Figs. 7(b) and 7(c), which shows that the atomic size misfit or γ_{USF} effects do not apply at low solute concentrations.

However, when the Mg concentration is >6 at. %, the MNW outer shell is largely occupied by Mg atoms, causing host-solute interactions to be significant. This triggers misfit and γ_{USF} effects. Al-Mg MNWs experience surface segregation of Mg atoms following hybrid MD/MC simulations, but no precipitates form in the examined range. In contrast, Mg-Al MNWs form surface/near surface precipitates when Al concentration is >8 at. %. These precipitates act as stress concentrators, decreasing the barrier for dislocation initiation at the interfaces between precipitates and bulk phases. Thus, surface/near surface clusters act as surface defects, making it easier for yielding behavior to activate, like that reported by Wu *et al.* [47] and Sharma *et al.* [26].

Zhu *et al.* [54] proposed two main factors, activation energy and activation volume, to be highly associated with the athermal part of the dislocation nucleation stress. The activation volume is proportional to b^3, where b is the Burgers vector length, which suggests it is related to the lattice constant of alloys. The addition of solute atoms can alter the lattice constant due to atomic size mismatch. Additionally, γ_{USF} can

be associated with the activation energy, which is the energy barrier of the dislocation nucleation. Compared with these two factors, evaluating γ_{USF} and atomic size misfit is a simpler approach to predicting the yield strength of single crystalline MNWs.

It is thought that the activation energy can be linked to γ_{USF}. When the atomic size misfit is not significant (e.g., Ni-Cu, NiFe-Cu, and CoCrNiFe-Cu MNWs), this energy has a major effect on the dislocation nucleation behavior. In these cases, the activation volume is not significantly altered; however, the activation energy can be drastically altered by increasing the solute concentration.

We believe that both the activation energy and the activation volume play significant roles in the surface dislocation nucleation of Cu-Ag and Ag-Cu MNWs, where atomic size mismatch dominates the softening phenomenon. The lattice mismatch can cause stress concentration, thus lowering the energy barrier for dislocation nucleation, especially at high concentrations. Even though the small addition of solute atoms may not have a huge effect on the activation energy or γ_{USF}, particularly in Ag-Cu MNWs (Table V), it can still significantly alter the lattice constant, indicating a major enlargement or reduction in activation volume.

D. Clustering-induced softening

As described by Bisht *et al.* [10], atomic friction can affect the dislocation motion after its first nucleation, which can lead to the transition from softening to strengthening in the Ni-Co alloy nanoparticles by increasing the solute Co concentration. However, this description does not explain the transition from softening to strengthening in the hybrid MD/MC-treated Ni-Co MNWs since the yielding happens when the nucleation of the first dislocation occurs, and no strain hardening can be observed, indicating that atomic friction cannot enhance the yield strength in this case. The atomic size misfit values for the Ni-Co alloy system, calculated by Eqs. (1) and (2), with atomic radii for Ni 124 pm and Co 125 pm taken from Ref. [53], show that the maximum atomic size misfit is < 0.4%. Thus, the atomic size misfit effects can be neglected for the Ni-Co alloy system.

The γ_{USF} values are increased with Co concentration until it reaches Co-50 at. %, followed by a slight decrease, as shown in Table III. Since γ_{USF} can be considered the partial dislocation nucleation energy barrier, the strengthening in Ni-Co MNWs can be attributed to the increase in γ_{USF} caused by adding more Co atoms. However, the Ni-Co alloy MNWs have been significantly softened after hybrid MD/MC simulations compared with their random condition, as illustrated by the colored region in Fig. 4(b). This softening can be attributed to the formation of Co clusters, which is evident in Fig. 8(b), as it can significantly reduce the host-solute interactions and form cluster-host interfaces, thereby decreasing the partial dislocation nucleation energy barrier. The result of this paper is in stark contrast to the findings of Cao [55] on polycrystal CrCoNi alloys, where the clusters acted as barriers to dislocation slip, resulting in an increase in the flow stress and therefore strengthening. In contrast, in this paper, we found that the clusters act as stress concentration and heterogeneous nucleation sites, which could lower the energy barrier for

(a)

(b)
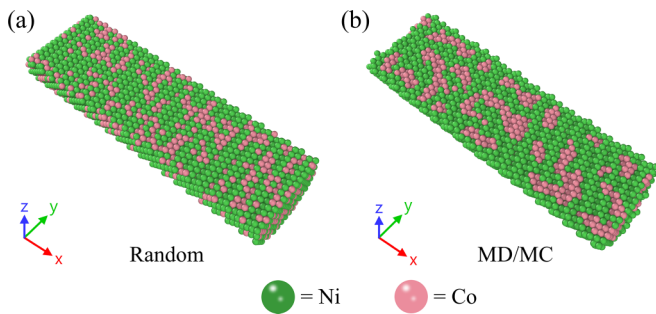
● = Ni   ● = Co

FIG. 8. Comparison of the solute Co distribution (a) in the random condition and (b) after hybrid molecular dynamics (MD)/Monte Carlo (MC) simulations in Ni-Co metal nanowires (MNWs).

dislocation nucleation and thus lead to softening in single crystalline MNWs. Thus, the transition between softening and strengthening in the Ni-Co alloy system can be explained by the competition of two opposite effects: solute clustering softens the partial dislocation nucleation energy barrier, and higher solute concentration enhances the γ_{USF} values, increasing the energy barrier of first partial nucleation.

It is worth noting that hybrid MD/MC relaxation also softens the Ag-Cu MNWs compared with their random counterparts, as seen in Fig. 4(c). Small Cu clusters have been formed after atomic swapping, as shown in Fig. 3(d). This softening can be attributed to clustering-induced softening, like that observed in Ni-Co MNWs with hybrid MD/MC relaxation.

E. Precipitation-induced softening

The focus of this paper is on SSS; however, precipitates can also cause softening effects in some scenarios. Sharma *et al.* [26] discovered Fe-rich precipitates on the surface and near the edges of the Ni-27Fe and Ni-50Fe dislocation-free nanoparticles. The existence of these precipitates can facilitate the nucleation of dislocations and induce softening. This precipitation-induced softening is distinct from the classical precipitation hardening due to the different yielding mechanisms; the former is yielded by dislocation nucleation, while the latter is yielded by dislocation motion. In this paper, similar precipitation-induced softening can also be seen in Mg-Al MNWs. After hybrid MD/MC relaxation, Al-rich phases (or precipitates) were formed, as demonstrated in Fig. 3(f). These precipitates facilitated dislocation nucleation at the surface sites, which in turn lowered the yield strength of the Mg-Al MNWs [Fig. 4(d)].

V. CONCLUSIONS

In conclusion, in this paper, we investigated the alloying-induced softening, particularly the SSS, in single crystalline MNWs in several alloy systems by atomistic simulations. The following main conclusions can be drawn:

(1) The alloying-induced softening phenomenon, particularly that caused by forming a solid solution, can be observed in defect-free single crystalline MNWs.

(2) SFE-induced softening and atomic size misfit-induced softening are two major sources that soften the alloy MNWs. Both affect the nucleation of the first partial dislocation and therefore the yielding behavior of single crystalline alloy MNWs.

(3) SFE dominates the SSS in Ni-Cu, NiFe-Cu MEA, and CoCrNiFe-Cu HEA MNWs, while atomic size misfit dominates the softening behavior in immiscible Cu-Ag MNWs. A misfit-SFE combined softening mechanism can be observed in Al-Mg MNWs.

(4) Solute clustering can also cause softening when the aforementioned mechanisms do not apply, e.g., in Ni-Co single crystalline MNWs.

[1] A. Sato and M. Meshii, Solid solution softening and solid solution hardening, Acta Metall. **21**, 753 (1973).

[2] R. J. Arsenault, The double-kink model for low-temperature deformation of B.C.C. metals and solid solutions, Acta Metall. **15**, 501 (1967).

[3] Q. Cheng, X. D. Xu, X. Q. Li, Y. P. Li, T. G. Nieh, and M. W. Chen, Solid solution softening in a Al$_{0.1}$CoCrFeMnNi high-entropy alloy, Scr. Mater. **186**, 63 (2020).

[4] M. P. Agustianingrum, Effect of aluminum addition on solid solution strengthening in CoCrNi medium-entropy alloy, J. Alloys Compd. **7**, 866 (2019).

[5] W.-R. Wang, W.-L. Wang, S.-C. Wang, Y.-C. Tsai, C.-H. Lai, and J.-W. Yeh, Effects of Al addition on the microstructure and mechanical property of Al$_x$CoCrFeNi high-entropy alloys, Intermetallics **26**, 44 (2012).

[6] M. S. Nitol, S. Adibi, C. D. Barrett, and J. W. Wilkerson, Solid solution softening in dislocation-starved Mg–Al alloys, Mech. Mater. **150**, 103588 (2020).

[7] N. I. Medvedeva, Yu. N. Gornostyrev, and A. J. Freeman, Electronic Origin of Solid Solution Softening in bcc Molybdenum Alloys, Phys. Rev. Lett. **94**, 136402 (2005).

[8] N. I. Medvedeva, Yu. N. Gornostyrev, and A. J. Freeman, Solid solution softening in bcc Mo alloys: Effect of transition-metal additions on dislocation structure and mobility, Phys. Rev. B **72**, 134107 (2005).

[9] N. I. Medvedeva, Yu. N. Gornostyrev, and A. J. Freeman, Solid solution softening and hardening in the group-V and group-VI bcc transition metals alloys: First principles calculations and atomistic modeling, Phys. Rev. B **76**, 212104 (2007).

[10] A. Bisht, R. K. Koju, Y. Qi, J. Hickman, Y. Mishin, and E. Rabkin, The impact of alloying on defect-free nanoparticles exhibiting softer but tougher behavior, Nat. Commun. **12**, 2515 (2021).

[11] Y.-J. Hu, M. R. Fellinger, B. G. Butler, Y. Wang, K. A. Darling, L. J. Kecskes, D. R. Trinkle, and Z.-K. Liu, Solute-induced

solid-solution softening and hardening in bcc tungsten, Acta Mater. **141**, 304 (2017).

[12] Y. Huo, J. Wu, and C. C. Lee, Solid solution softening and enhanced ductility in concentrated FCC silver solid solution alloys, Mater. Sci. Eng.: A **729**, 208 (2018).

[13] T. Tsuru, Y. Udagawa, M. Yamaguchi, M. Itakura, H. Kaburaki, and Y. Kaji, Solution softening in magnesium alloys the effect of solid solutions on the dislocation core structure and nonbasal slip, J. Phys.: Condens. Matter **25**, 022202 (2012).

[14] J. Diao, K. Gall, and M. L. Dunn, Yield strength asymmetry in metal nanowires, Nano Lett. **4**, 1863 (2004).

[15] H. Pan, W. Chen, Y. P. Feng, W. Ji, and J. Lin, Optical limiting properties of metal nanowires, Appl. Phys. Lett. **88**, 223106 (2006).

[16] W. Liang, M. Zhou, and F. Ke, Shape memory effect in Cu nanowires, Nano Lett. **5**, 2039 (2005).

[17] R. Rezaei and C. Deng, Pseudoelasticity and shape memory effects in cylindrical FCC metal nanowires, Acta Mater. **132**, 49 (2017).

[18] B. H. Hong, S. C. Bae, C.-W. Lee, S. Jeong, and K. S. Kim, Ultrathin single-crystalline silver nanowire arrays formed in an ambient solution phase, Science **294**, 348 (2001).

[19] J. Xu and Y. Xu, Fabrication and magnetic property of binary Co–Ni nanowire array by alternating current electrodeposition, Appl. Surf. Sci. **253**, 7203 (2007).

[20] S. Kar, T. Ghoshal, and S. Chaudhuri, Simple thermal evaporation route to synthesize Zn and Cd metal nanowires, Chem. Phys. Lett. **419**, 174 (2006).

[21] D.-G. Xie, Z.-Y. Nie, S. Shinzato, Y.-Q. Yang, F.-X. Liu, S. Ogata, J. Li, E. Ma, and Z.-W. Shan, Controlled growth of single-crystalline metal nanowires via thermomigration across a nanoscale junction, Nat. Commun. **10**, 4478 (2019).

[22] K. K. Kim, S. Hong, H. M. Cho, J. Lee, Y. D. Suh, J. Ham, and S. H. Ko, Highly sensitive and stretchable multidimensional strain sensor with prestrained anisotropic metal nanowire percolation networks, Nano Lett. **15**, 5240 (2015).

[23] K. Zhang, K. Han, S. Shi, G. Bahl, and S. Tawfick, Highly stretchable conductors made by laser draw-casting of ultralong metal nanowires, Adv. Electron. Mater. **2**, 1600003 (2016).

[24] H. Zhang, Y. Tian, S. Wang, J. Feng, C. Hang, C. Wang, J. Ma, X. Hu, Z. Zheng, and H. Dong, Robust Cu-Au alloy nanowires flexible transparent electrode for asymmetric electrochromic energy storage device, Chem. Eng. J. **426**, 131438 (2021).

[25] J. Yang, F. Yu, A. Chen, S. Zhao, Y. Zhou, S. Zhang, T. Sun, and G. Hu, Synthesis and application of silver and copper nanowires in high transparent solar cells, Adv. Powder Mater. **1**, 100045 (2022).

[26] A. Sharma, O. Mendelsohn, A. Bisht, J. Michler, R. K. Koju, Y. Mishin, and E. Rabkin, Solid-solution and precipitation softening effects in defect-free faceted nickel-iron nanoparticles, Acta Mater. **243**, 118527 (2023).

[27] X. Zhang, H. Deng, S. Xiao, X. Li, and W. Hu, Atomistic simulations of solid solution strengthening in Ni-based superalloy, Comput. Mater. Sci. **68**, 132 (2013).

[28] S. Plimpton, Fast parallel algorithms for short-range molecular dynamics, J. Comput. Phys. **117**, 1 (1995).

[29] P. Hirel, Atomsk: A tool for manipulating and converting atomic data files, Comput. Phys. Commun. **197**, 212 (2015).

[30] A. Stukowski, Visualization and analysis of atomistic simulation data with OVITO–The open visualization tool, Modelling Simul. Mater. Sci. Eng. **18**, 015012 (2009).

[31] A. Stukowski, Structure identification methods for atomistic simulations of crystalline materials, Modelling Simul. Mater. Sci. Eng. **20**, 045021 (2012).

[32] A. Stukowski, V. V. Bulatov, and A. Arsenlis, Automated identification and indexing of dislocations in crystal interfaces, Modelling Simul. Mater. Sci. Eng. **20**, 085007 (2012).

[33] V. Dupont and F. Sansoz, Molecular dynamics study of crystal plasticity during nanoindentation in Ni nanowires, J. Mater. Res. **24**, 948 (2009).

[34] W. Wang, C. Yi, and K. Fan, Molecular dynamics study on temperature and strain rate dependences of mechanical tensile properties of ultrathin nickel nanowires, Trans. Nonferrous Met. Soc. China **23**, 3353 (2013).

[35] B. Onat and S. Durukanoğlu, An optimized interatomic potential for Cu–Ni alloys with the embedded-atom method, J. Phys.: Condens. Matter **26**, 035404 (2014).

[36] G. P. Purja Pun, V. Yamakov, and Y. Mishin, Interatomic potential for the ternary Ni–Al–Co system and application to atomistic modeling of the B2-L1$_0$ martensitic transformation, Modelling Simul. Mater. Sci. Eng. **23**, 065006 (2015).

[37] P. L. Williams, Y. Mishin, and J. C. Hamilton, An embedded-atom potential for the Cu–Ag system, Modelling Simul. Mater. Sci. Eng. **14**, 817 (2006).

[38] O. R. Deluigi, R. C. Pasianot, F. J. Valencia, A. Caro, D. Farkas, and E. M. Bringa, Simulations of primary damage in a high entropy alloy: Probing enhanced radiation resistance, Acta Mater. **213**, 116951 (2021).

[39] D. H. Tsai, The virial theorem and stress calculation in molecular dynamics, J. Chem. Phys. **70**, 1375 (1979).

[40] M. I. Mendelev, M. Asta, M. J. Rahman, and J. J. Hoyt, Development of interatomic potentials appropriate for simulation of solid–liquid interface properties in Al–Mg alloys, Philos. Mag. **89**, 3269 (2009).

[41] B. Sadigh, P. Erhart, A. Stukowski, A. Caro, E. Martinez, and L. Zepeda-Ruiz, Scalable parallel Monte Carlo algorithm for atomistic simulations of precipitation in alloys, Phys. Rev. B **85**, 184203 (2012).

[42] H. J. C. Berendsen, J. P. M. Postma, W. F. van Gunsteren, A. DiNola, and J. R. Haak, Molecular dynamics with coupling to an external bath, J. Chem. Phys. **81**, 3684 (1984).

[43] J. A. Zimmerman, H. Gao, and F. F. Abraham, Generalized stacking fault energies for embedded atom FCC metals, Modelling Simul. Mater. Sci. Eng. **8**, 103 (2000).

[44] C. Deng and F. Sansoz, Fundamental differences in the plasticity of periodically twinned nanowires in Au, Ag, Al, Cu, Pb and Ni, Acta Mater. **57**, 6090 (2009).

[45] J. Xiao and C. Deng, Continuous strengthening in nanotwinned high-entropy alloys enabled by martensite transformation, Phys. Rev. Mater. **4**, 043602 (2020).

[46] See Supplemental Material at http://link.aps.org/supplemental/10.1103/PhysRevMaterials.7.053611 for additional details about the SFE calculation results of the Ni-Cu system with orderly distributed Cu atoms; the softening behavior in Ni-Cu MNWs with different strain rates and temperatures; and structures of Al-Mg MNWs after hybrid MD/MC simulations for low- and high-solute concentrations.

[47] Z. X. Wu, Y. W. Zhang, M. H. Jhon, J. R. Greer, and D. J. Srolovitz, Nanostructure and surface effects on yield in Cu nanowires, Acta Mater. **61**, 6 (2013).

[48] S. M. Foiles, Calculation of the surface segregation of Ni-Cu alloys with the use of the embedded-atom method, Phys. Rev. B **32**, 7685 (1985).

[49] T. Sakurai, T. Hashizume, A. Jimbo, A. Sakai, and S. Hyodo, New Result in Surface Segregation of Ni-Cu Binary Alloys, Phys. Rev. Lett. **55**, 514 (1985).

[50] D. J. Siegel, Generalized stacking fault energies, ductilities, and twinnabilities of Ni and selected Ni alloys, Appl. Phys. Lett. **87**, 121901 (2005).

[51] Y. Mishin, M. J. Mehl, D. A. Papaconstantopoulos, A. F. Voter, and J. D. Kress, Structural stability and lattice defects in copper: *Ab initio*, tight-binding, and embedded-atom calculations, Phys. Rev. B **63**, 224106 (2001).

[52] Y. Zhang, X. Yang, and P. K. Liaw, Alloy design and properties optimization of high-entropy alloys, JOM **64**, 830 (2012).

[53] N. N. Greenwood and A. Earnshaw, *Chemistry of the Elements* (Elsevier, Oxford, 1997).

[54] T. Zhu, J. Li, A. Samanta, A. Leach, and K. Gall, Temperature and Strain-Rate Dependence of Surface Dislocation Nucleation, Phys. Rev. Lett. **100**, 025502 (2008).

[55] P. Cao, Maximum strength and dislocation patterning in multi–principal element alloys, Sci. Adv. **8**, eabq7433 (2022).